analytical chemistry

Article

Quantum Dots Based Fluorescent Traffic Light Nanoprobe for Specific Imaging of Avidin-Type Biotin Receptor and Differentiation of Cancer Cells

Haojun Jin, Qian Jin, Zhenghui Liang, Yuqian Liu, Xiaojun Qu, and Qingjiang Sun

Anal. Chem., **Just Accepted Manuscript** • DOI: 10.1021/acs.analchem.9b00924 • Publication Date (Web): 19 Jun 2019

Just Accepted

is published by the American Chemical Society. 1155 Sixteenth Street N.W., Washington, DC 20036

Quantum Dots Based Fluorescent Traffic Light Nanoprobe for Specific Imaging of Avidin-Type Biotin Receptor and Differentiation of Cancer Cells

Haojun Jin,† Qian Jin,‡ Zhenghui Liang,† Yuqian Liu,† Xiaojun Qu,† and Qingjiang Sun*,†

†State Key Laboratory of Bioelectronics, School of Biological Science & Medical Engineering, Southeast University, Nanjing 210096, China

‡601 W, 115th St, New York, NY 10025, United States

*Fax: (86) 25-83792349. Email: sunqj@seu.edu.cn

ABSTRACT: Sensitive and specific visualization of cell surface biotin receptors (BRs), a clinical important biomarker, remains a challenge. In this work, a dual emission ratiometric fluorescent nanoprobe is developed for specific imaging of cell surface avidin, a subtype of BRs. The nanoprobe comprises a dual emission quantum dots nanohybrid, wherein a silica-encapsulated red-emission QD (rQD@SiO_2) is used as "core" and green-emission QDs (gQDs) are used as "satellites", which are further decorated with new "love-hate"-type BR ligand, a phenanthroline-biotin conjugate with an amino linker. The nanoprobe shows intense rQD emission but quenched gQD emission by the BR ligand. Upon imaging, the rQD emission stays constant and the gQD emission restores as cell surface avidin accrues. Accordingly, the overlaid fluorescence color collected from red and green emission changes from red to yellow, and then to green. We refer to such color change as a traffic light pattern and the nanoprobe as fluorescent traffic light nanoprobe. We demonstrate the application of our fluorescent traffic light nanoprobe to characterize cancer cells. By the traffic light pattern, cervical carcinoma and normal cells, as well as different-type cancer cells including BR-negative colon cancer cells, BR-positive hepatoma carcinoma cells, breast cancer cells and their subtypes have been visually differentiated. We further demonstrate a use of our nanoprobe to distinguish the G2 phase from other stages in a cell cycle. These applications provide new insights into visualizing cell surface biomarkers with remarkable imaging resolution and accuracy.

INTRODUCTION

Cell surface receptors are protein receptors embedded in cell membranes. They play key roles in a variety of physiological and pathological events.[1,2] Importantly, cell surface receptors are involved in progression of degenerative diseases, for instance, cancer, atherosclerosis, and neurological disorder.[3] Traditional detection methods of cell surface receptors include radiometric assay[4] and flow cytometry.[5] They either require cell invasion or do not provide imaging data to visually represent proteins on cell surfaces. The fluorescent probe-based imaging method provides an alternative to detect cell surface receptors with advantages in terms of real-time imaging, minimal invasiveness and high spatial resolution.[6,7] Scientists have synthesized a pool of fluorescent probes to visualize cell-surface receptors such as epidermal growth factor receptors and folate receptors.[8-11] Semi-quantitative fluorescence imaging methods have thus been developed for cancer diagnosis at early stage.[12,13]

Biotin receptors (BRs) are a class of cell surface receptors necessary for natural growth of living cells.[14] In order to rapidly proliferate, cancer cells overexpress BRs to acquire more biotins than normal cells. For certain cancer cell lines, the overexpression profiles of BRs are more pronounced than folate receptors.[15,16] Therefore, BRs have been recognized as a promising biomarker for cancer diagnosis and therapy.[17] Although efforts have been made to design fluorophore-biotin conjugates to image cell surface BRs, none of these probes seems to resolve the problems brought by systemic errors involved in the imaging process.[18-21] Their single-emission fluorescence signals are easily affected by systematic errors originated from variations in excitation intensity, local probe concentration, and cell microenvironment.[22] A dual emission ratiometric method could offset these systematic interferences, by including one emission from an internal standard at a wavelength and the other emission from the target at a second wavelength.[23,24] The overlaid fluorescence color obtained from dual emission can be used to precisely image the target.

Another challenge in imaging cell surface BRs involves selection of fluorophore-biotin conjugates. As for a fluorophore- biotin conjugate with a short linker, biotin moiety may quench the emission of fluorophore in close proximity, resulting in poor sensitivity.[25] With a long linker, the high affinity binding between a population of BRs and the conjugate may reduce the imaging specificity.[26] As a result, the subtypes (avidin and streptavidin) of BRs may not be differentiated.

Instead of a molecular probe, we hereby report a ratiometric fluorescent nanoprobe to image cell surface BRs. Our nanoprobe comprises a "core-satellite" dual emission QDs nanohybrid with specifically designed BR ligand, a phenanthroline-biotin conjugate (herein abbreviated as **PB**). **PB** binds to gQDs via metal affinity coordination and quenches the green emission by charge transfer. The nanoprobe provides a dual emission feature: red emission from CdSe/ZnS QD (rQD) inside silica shell is used as the internal reference, while green emission from InP/ZnS QDs (gQDs) outside of the silica shell is target-responsive (**Scheme 1**). Relying on molecular feature of **PB**, our nanoprobe can selectively recognize cell surface avidin (AV) rather than its isoform streptavidin (SA). The cell surface AV, when binding the biotin end of **PB**, can displace **PB** from the nanoprobe and restore the green emission. As a result, the dual emission (restored green emission and constant red emission) produces ratiometric fluorescence response of the nanoprobe. This ratiometric fluorescence response results in a change in the overlaid color of cell surface from red to yellow, and then to green, as the AV abundance increases. We refer to such color change as a traffic light pattern and the nanoprobe as fluorescent traffic light nanoprobe. This traffic light nanoprobe is demonstrated below to image living cell surfaces to differentiate cell status, types/subtypes and stages at a molecular level.

Scheme 1. Illustration of the nanoprobe construction and its use for imaging cell surface BRs.

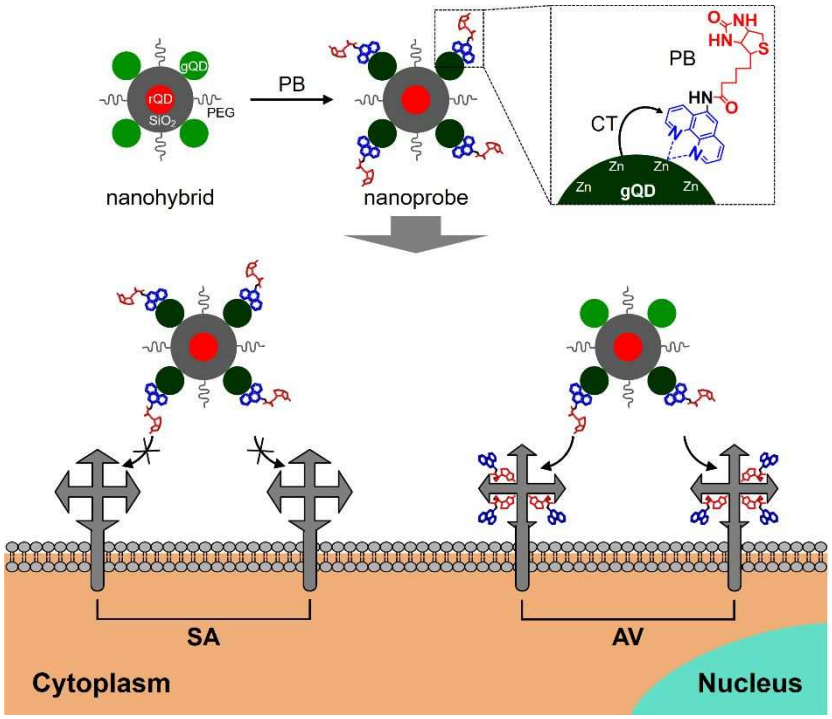

EXPERIMENTAL SECTION

Reagents and Chemicals. 1-Butanol, 5-amino-phenanthroline were supplied by Alfa Aesar. Thionyl chloride and cysteine (Cys) were purchased from Aladdin. AV, SA, pepsin, bovine serum albumin (BSA), thrombin (TB) and RNase A were purchased from Sigma-Aldrich. Biotin and 4-dimethylaminopyridine were purchased from TCI. N,N-dimethylformamide (DMF) and Glutathione (GSH) were purchased from J&K. Methoxy-poly(ethylene glycol)-monocarboxylic acid ($mPEG_{2000}$-COOH) was purchased from ToYong Bio. Co. Ltd. (Shanghai, China). The pure water (ρ> 18.2 MΩ cm) was obtained from a Pall Cascade AN synthesis system.

Synthesis of PB. PB was synthesized with a modified procedure.[27] Typically, 0.22 g of biotin was dissolved in 10 mL of thionyl chloride with stirring for 20 min to obtain biotin acyl chloride. In parallel, 0.20 g of 5-amino-phenanthroline and 0.02 g of 4-dimethylaminopyridine were dissolved in 15 mL of dry DMF, to which the biotin acyl chloride in 10 mL of DMF was transferred. The reaction was allowed to stir for 18 h at room temperature. The product was purified by alumina chromatography. 0.24 g of **PB** was obtained in a yield of 63%. ^{1}H NMR [$(CD_3)_2SO$]: δ 10.70 (1H, s), 9.12 (1H, dd), 9.03 (1H, dd), 8.60 (1H, d) 8.45 (1H, d), 8.16 (1H, s), 7.82 (1H, dd), 7.74 (1H, dd), 6.44 (1H, s), 6.36 (1H, s), 4.32 (1H, m), 4.17 (1H, m), 3.17 (1H, m), 2.83 (1H, m), 2.59 (1H, m), 1.72-1.48 (8H, m).

Preparation of the QDs Nanohybrid. The synthesis of water soluble mercaptopropionic acid-capped gQD (InP/ZnS, EM: 519 nm) and oil soluble rQD (CdSe/ZnS, EM: 619 nm) were described previously.[28,29] The silica encapsulated rQD (rQD@SiO_2) were prepared by a reverse microemulsion approach,[30] and further functionalized with $mPEG_{2000}$-COOH via typical carbodiimide reaction. The QDs nanohybrid was prepared by dropwise adding 0.5 μM of gQD into 0.03 μM of PEGylated rQD@SiO_2 with stirring for 20 min.

Preparation and Characterization of the Nanoprobe. The nanoprobe was prepared via a phase transfer process.[31] Typically, Tris-HCl buffer (10 mM, pH 7.4) of the QDs nanohybrid was mixed with 1 equiv. of 1-butanol solution of **PB** (10 μM), followed by shaking for 2 min. After a 10-minute standing, the two solutions in the cuvette were stratified, and the aqueous solution was stored for further use.

The photostability was characterized by illuminating the nanoprobe in Tris-HCl buffer with a laser at 405 nm for different time (up to 2 h), followed by fluorescence measurements. The biocompatibility was characterized by incubating HeLa cells with varying concentrations of the nanoprobe for 24 h, and subsequent staining with (3-(4,5-dimethyl-2-thiazolyl)-2,5-diphenyl-2-H-tetrazolium bromide) (MTT) for 4 h, followed by absorption measurements.

Fluorescence Measurements. All the fluorescence measurements were conducted with a 0.2 cm-thick quartz cuvette, an excitation wavelength at 405 nm and a 5 nm slit. For sensitivity assessment, solutions of the nanoprobe were equally mixed with varying concentrations of AV. For selectivity assessment, solutions of the nanoprobe were equally mixed with solutions of 0.2 μM of AV, SA, pepsin, BSA, TB or RNase A, or 0.1 mM of GSH or Cys, respectively. For competitive binding experiment, solutions of the nanoprobe were mixed with 0.2 μM of AV, followed by the addition of 0, 0.1 or 0.2 μM of biotin-C-peptide, respectively.

Docking Calculations. The structure of **PB** was optimized by Gaussian 03 at HF/3-21G level of calculation. The crystallographic structures of AV and SA were obtained from the Protein Data Bank (https://www.wwpdb.org). The standard protocol of merging hydrogens, assigning Gasteiger charges and AutoDock atom types, was followed to prepare ligand and protein input files. Docking calculations were performed by using the AutoDock v4.2 (https://autodock.scripps.edu) and AutoDockTools ADT v1.5.6 (https://mgltools.scripps.edu).[32,33] The docking grid size was set to 60×60×60 points with grid

spacing of 0.375 Å, which embraces the binding sites of the proteins. The docking utilized the standard AutoDock force field and the Lamarckian Genetic Algorithm (LGA) search for the lowest energy docked ligand conformers. Each docking calculation consisted of 10 independent LGA runs with the maximum number of energy evaluations for each LGA run set at 2 500 000 with the generations set to a maximum of 27 000. The resulting docking poses were analyzed based on their AutoDock binding energies.

Cell Surface Imaging. Cell imaging was carried out after the nanoprobe-treated cells were washed with PBS, and fixed with paraformaldehyde on Lab-Tek 8 well chambered coverglass. Green-channel (509-529 nm) and red-channel (609-629 nm) emissions were collected, respectively, upon laser excitation at 405 nm. The fluorescence images were quantitatively analyzed using the ImageJ software (https://imagej.nih.gov/ij/). Fluorescence colors of the overlaid images were also analyzed.

To study the kinetics of imaging, HeLa cells were pre-stained with a plasma membrane dye, DiD [$DiIC_{18}(5)$], and then treated with 0.05, 0.15 and 0.25 mg/mL of the nanoprobe for 1, 2, 4, 6 and 8 h, respectively. The reference red emission of the nanoprobe was monitored to indicate its localization on cell surfaces. To study the specificity of imaging, HeLa cells were pre-incubated with 0.5 μM of AV or SA for 12 h, or 10 μM of biotin for 1 h, followed by treating with the nanoprobe (0.15 mg/mL, thereafter) for 6 h. To differentiate normal/cancer cells, Ect1/E6E7 cells and HeLa cells were, respectively, treated with the nanoprobe for 6 h. To differentiate cancer cell types/subtypes, HCT116 cells, MDA-MB-231 cells, SKBr3 cells and HepG2 cells were, respectively, treated with the nanoprobe for 6 h. To image the stages during a cell cycle, HeLa cells were pre-incubated with 200 nM of L-mimosine for 24 h (G1 phase), 2 mM of thymidine for 24 h (S phase), 3 μM of nocodazole for 24 h (G2 phase), as well as 2 mM of thymidine for 18 h and 0.3 μM of nocodazole for 12 h (M phase), respectively, followed by treating with the nanoprobe for 6 h.

Instruments. Fluorescence spectra were collected with a fluorescence spectrometer (Hitachi F-7000, Japan). UV/Vis absorption spectra were acquired on a Hitachi U-4100 spectrophotometer. The ^{1}H NMR spectrum was recorded on a Bruker DRX-400 NMR spectrometer. Fourier transform infrared (FT-IR) spectra were obtained on a Thermo Scientific Nicolet-5700 spectrometer. X-ray photoelectron spectroscopy (XPS) was acquired from a PHI 5000 VersaProbe spectrometer (ULVAC-PHI, Inc.) equipped with a monochromatic Al Kα source at room temperature. Zeta potential measurements were performed on a Malvern Zetasizer Nano-ZS particle analyzer. Transmission electron microscopy (TEM) images were taken on a JEOL JEM-2100 microscope. Confocal fluorescence images were taken on a confocal laser-scanning microscope (TCS SP8, Leica, Germany).

RESULTS AND DISCUSSION

Preparation and Characterization of the Nanoprobe. The nanoprobe was assembled by a two-step adsorption process. At first step, mercaptopropionic acid-capped gQDs were adsorbed onto an amino-modified PEGylated rQD@SiO_2 via electrostatic interaction to form a QDs nanohybrid. The TEM image shows that the nanohybrid has a well-defined "core-satellite" structure, in which one rQD (d = 7.5 nm) is embedded within a ~17 nm-thick silica shell and multiple gQDs (d = 3.3 nm) are anchored on the surface of silica shell (Figure 1A). The thickness of silica shell well exceeds the Förster radius (~5-7 nm),[34,35] thereby blocking resonance energy transfer between the rQD and the gQDs. In accordance with the electrostatic adsorption, ζ potential drastically changes from 18.4 mV for rQD@SiO_2 to -22.6 mV for the QDs nanohybrid (Figure S1).

At second step, the ligand **PB** was adsorbed onto gQDs of the QDs nanohybrid by metal affinity coordination. This coordination was confirmed by the findings that a band peaked at 397.1 eV for N 1s signal and another band peaked at 1020 eV for Zn $2p_{3/2}$ signal appear in the XPS spectrum of nanoprobe with respect to that of the QDs nanohybrid (Figure 1B, a,b). These results indicate that the coordination takes place between two N atoms on phenanthroline moiety of **PB** and surface Zn atoms of gQDs (InP/ZnS).[36,37] It is worth noting that **PB** is virtually insoluble in water. Therefore, the **PB**/gQD binding was via a phase transfer approach, by which eight **PB** molecules can be adsorbed onto one gQD (Figure S2). At this **PB**/gQD ratio, the nanoprobe shows intense rQD emission and weak gQD emission (quenched to be one fifth of the original), making the overlaid fluorescence color show red (Figure 1C).

The photostability of the dual emission nanoprobe is further evaluated. Both the gQD emission and the rQD emission are found to slowly bleach upon continuous laser illumination, but they exhibit nearly identical photo-bleaching behavior (Figure S3). As a result, the dual emission based fluorescence ratiometry remains nearly constant, indicative of high detection accuracy by the nanoprobe.

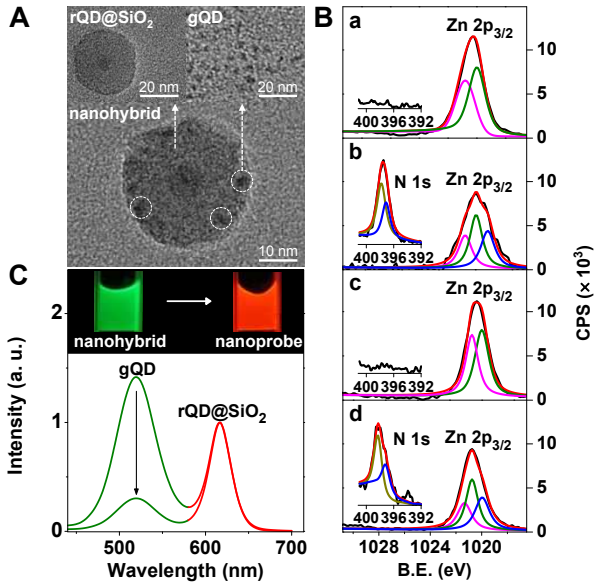

Figure 1. (A) TEM images of rQD@SiO_2, gQD, and the QDs nanohybrid. (B) XPS spectra of the QDs nanohybrid (a), the nanoprobe (b), and the nanoprobe in the presence of AV (c) or SA (d). Spectral components of N 1s are N-C (yellow) and N-Zn (blue). Spectral components of Zn $2p_{3/2}$ are Zn-O (pink), Zn-S (green) and Zn-N (blue). (C) Fluorescence spectra and photographs of the QDs nanohybrid and nanoprobe solutions.

Sensitivity Assessment of the Nanoprobe in a Test Tube Setting. The nanoprobe is initially tested by free AV which binds biotin in the same way as cell surface AV.[38] As shown in Figure 2A, the nanoprobe exhibits a ratiometric fluorescent response to a dose range of AV. Increasing the AV concentration results in stronger gQD emission at 519 nm (I_{519}), while the rQD emission at 619 nm (I_{619}) remains

constant. The relative green-to-red emission intensity ratio displays a linear correlation with the AV concentration in the range of 0.1-100 nM, with a correlation coefficient of 0.991 (Figure 2B). The limit of detection can be defined as 0.1 nM. From the linear correlation, the apparent dissociation constant (K_d) of **PB** is calculated to be 7.5×10^{-8} M, which is 10^6-10^7-fold larger than that of free biotin (~10^{-15} M).

More importantly, under UV illumination, the nanoprobe solution displays a color change from red to yellow and then to green, as AV concentration increases (Figure 2, top). The color change is analogous to that of a traffic light. We refer to such color change as a traffic light pattern: the red light is on when the AV concentration is no more than 10 nM; the yellow light makes transitions when the AV concentration is in the range of 25-50 nM; the green light is on when the AV concentration is greater than 60 nM. Clearly, this traffic light pattern facilitates to visualize AV in a semi-quantitative manner.

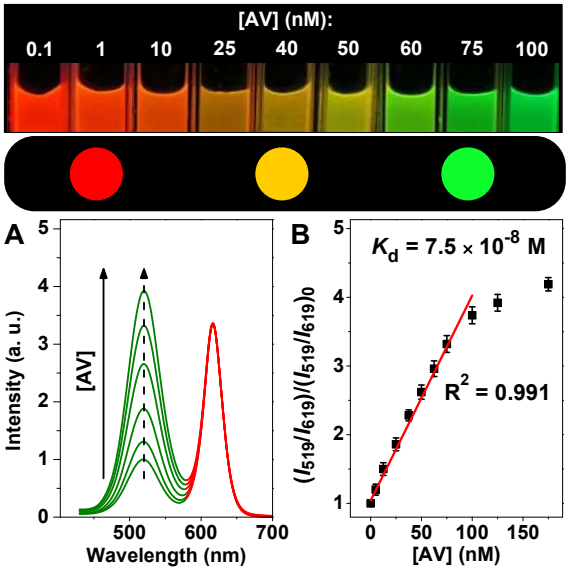

Figure 2. (Top) Photographs of the nanoprobe in a test tube setting as AV concentration increases. (Middle) The traffic light pattern represents the overlaid fluorescence color of the nanoprobe at different concentration ranges of AV. (A) Fluorescence spectra of the nanoprobe (0.15 mg/mL) in the presence of varying concentrations of AV. (B) Relative green-to-red emission intensity ratio as a function of AV concentration. The error bars represent the relative error propagated for green-to-red emission intensity ratios for three replicated measurements.

Specificity Assessment of the Nanoprobe for BRs. To investigate the specificity of the nanoprobe, the nanoprobe is treated with a variety of proteins, i.e., AV (model target for AV-type BRs), SA (model target for SA-type BRs), pepsin, BSA, TB and RNase A, and biothiols (GSH and Cys). The relative green-to-red emission intensity ratio is examined for each of the proteins/biothiols. We find that our nanoprobe is specific for AV only. AV displays larger relative green-to-red emission intensity ratio than SA by a factor of ~10-fold (Figure 3). The change in fluorescence ratiometry induced by other proteins/biothiols is negligible. The specificity of the nanoprobe toward AV versus SA is further confirmed by other spectral measurements. When AV is present, **PB** is displaced from the gQDs characterized by all nitrogen band peaks disappearing in the XPS spectrum (Figure 1B, c). As for SA, it does not dislocate **PB** from the nanoprobe (Figure 1B, d). FT-IR spectra also show that characteristic vibration bands for **PB** (2973 cm^{-1} for alkyl group; 1660 cm^{-1} for amide group) disappear from the nanoprobe in the presence of AV, while these bands still exist in the presence of SA (Figure S4).

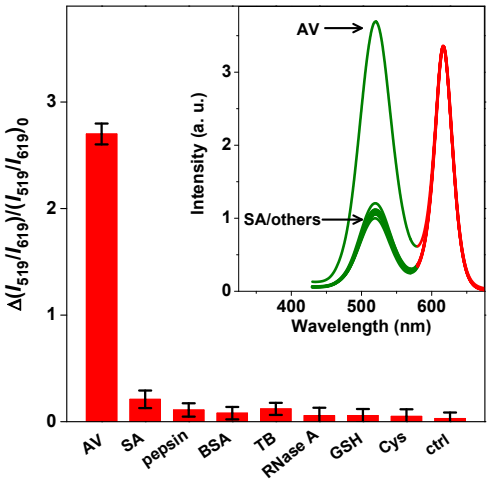

Figure 3. Histogram of relative green-to-red emission intensity for the nanoprobe (0.15 mg/mL) in the presence of 0.1 μM of proteins (AV, SA, pepsin, BSA, TB, or RNase A), or 0.05 mM of biothiols (GSH or Cys). The error bars represent the relative error propagated for green-to-red emission intensity ratios for three replicated measurements. The inset shows the corresponding fluorescence spectra.

Ligand-Governed Specificity of the Nanoprobe toward AV. To obtain insights into the specificity of the nanoprobe, docking studies for **PB**-AV monomer and **PB**-SA monomer are performed using AutoDock program. The calculations show that **PB** can bind AV, with the biotin end (red) inside the binding pocket and the phenanthroline arm (blue) nearby the protein surface (Figure 4A, left). This configuration of **PB**-AV complex is similar to that of other biotin conjugate-AV complexes.[39,40] In contrast, **PB** may not access into the binding pocket of SA regardless of dimensional adjustment (Figure 4A, right).

The difference in binding may be attributable to the conformation of critical loop at the surface of proteins. For AV and SA, three polypeptide loops (L3-4, L5-6 and L7-8) cover their binding pockets, among which L3-4 (connect strands β3 to β4) is regarded to play a critical role in ligand binding. This critical loop contains nine residues in AV but only six residues in SA.[41-43] Therefore, L3-4 of AV is larger and more flexible than that of SA. The lid-like loop L3-4 of AV may adopt an openable conformation, whereas L3-4 of SA has a closed conformation upon ligand binding.[44,45]

The steric structure of the ligand **PB** also contributes to the specific binding. **PB** features a "love-hate" structure[46]: on one hand, it has a biotin end that favors high-affinity binding with the pocket of AV or SA ("love" mode); on the other hand, **PB** has a rigid phenanthroline arm that sterically clashes with the surface of proteins ("hate" mode). The flexible open conformation of L3-4 in AV may enhance the "love" mode and suppress the "hate" mode, which results in binding between **PB** and AV (Figure 4B, left). In contrast, the closed conformation of L3-4 in SA enhances the "hate" mode, restricting the binding of **PB** with SA (Figure 4B, right).

Additionally, we study the fluorescence of the AV pre-treated nanoprobe in the presence of a binding competitor, i.e., biotin-C-peptide. Biotin-C-peptide shares the same biotin end, but has longer (7-atom) linker and much larger arm (C-peptide) than **PB**. As illustrated in Figure S5, the restored green

emission of nanoprobe by the presence of AV is quenched again with the addition of biotin-C-peptide. This result indicates that biotin-C-peptide competes with **PB,** and displaces it from the binding pocket of AV. The higher affinity binding of biotin-C-peptide than **PB** may be attributed to the fact that the 7-atom linker allows the bulky C-peptide arm away from protein surface without generating the steric clash.[46,47] Consequently, the "hate" mode of the ligand is suppressed. Together the results suggest that the "love-hate" mode governs the specific ligand/protein binding. For **PB**, the balance between the dual modes reduces its binding affinity (K_d of **PB** >> that of free biotin), but improves its binding specificity (AV versus SA).

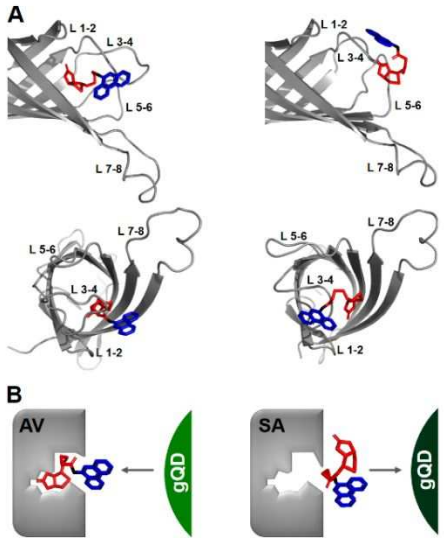

Figure 4. (A) Side view and top view that depict the docking of a **PB** molecule toward AV monomer (left) and SA monomer (right). (B) Illustration of the specificity of the nanoprobe toward AV versus SA.

Ratiometric Imaging of Cell Surface AV and Differentiation of Normal/Cancer Cells. The nanoprobe is used to examine BR-positive HeLa cell line. Prior to cell imaging, biocompatibility of the nanoprobe is evaluated. The MTT assay reveals that up to 0.25 mg/mL of the nanoprobe has a negligible effect on cell viability in 24 h incubation, indicative of low cytotoxicity of the nanoprobe (Figure S6). Furthermore, kinetics for cell imaging is conducted by fluorescence co-localization experiments. The cell membranes are pre-stained with a dye DiD, and the reference rQD emission of the nanoprobe is used to indicate its localization on cell surfaces. As shown in Figure S7, at a concentration of 0.05 mg/mL, the nanoprobe cannot be localized on entire cell surface even after 8 h incubation, displaying the weak red emission. At higher concentrations of 0.15 and 0.25 mg/mL, the nanoprobe can be localized on entire cell surface by 6 h treatment, showing the intense red emission which overlaps with that of DiD. With 8 h incubation at such concentrations, the nanoprobe can partially enter into the cell plasma. These results suggest that a 6 h treatment with 0.15 mg/mL of the nanoprobe is preferential for cell surface imaging.

Figure 5 shows the confocal microscopy images of HeLa cells treated by the nanoprobe at the preferential condition. The red channel images demonstrate localization of nanoprobe on cell surfaces, and the green channel images are associated with abundances of BRs. While the relative green-to-red emission intensity ratio for the original nanoprobe is 0.3:1, the native Hela cells (first column) exhibit a much higher relative green-to-red emission intensity ratio of 0.8:1, which indicates the presence of BRs on cell surface. Further, the images of native HeLa cells are compared with those of AV- and biotin-pretreated HeLa cells. AV-pretreated HeLa cells have enriched AV-type BRs on the cell surfaces and the biotin-pretreated Hela cells have biotins that already bound to cell surface BRs. For AV-pretreated HeLa cells, the red channel emission intensity remains the same, while green channel emission intensity increases relative to that of the native cells, and the relative green-to-red emission intensity ratio increases to 1.4:1 (second column). In contrast, for biotin-pretreated cells, the green channel emission intensity was suppressed relative to that of native cells, and the relative green-to-red emission intensity ratio becomes 0.3:1, identical to that of the original nanoprobe (third column).

Alternative to quantification by green channel and red channel emission intensities, a more convenient method to assess the abundance of cell surface BRs is examination of the dual emission overlaid color, i.e., ratiometric fluorescence imaging by the nanoprobe. For AV-pretreated, native, and biotin-pretreated HeLa cells, cell surfaces show overlaid green light, yellow light, and red light, respectively. The traffic light pattern of the overlaid color indicates that our ratiometric fluorescent nanoprobe features semi-quantification of cell surface BRs with remarkable imaging resolution.

To assess the imaging specificity, the images of SA-pretreated HeLa cells (fourth column) are compared with those of native and AV-pretreated HeLa cells. The SA pretreatment enriches SA-type BRs on the cell surface. Despite this, the overlaid image of SA-pretreated HeLa cells also shows a yellow light, with the relative green-to-red emission intensity nearly identical to that for the native cells. These results indicate that only AV-type BRs are specifically visualized on cell surfaces by the nanoprobe, in consistency with the specificity toward free AV in the test tube setting.

On the basis of sensitivity and specificity, the nanoprobe is further used to examine normal cervical (Ect1/E6E7) cells. For Ect1/E6E7 cells, the green channel emission intensity was suppressed relative to that of HeLa cells, and the relative green-to-red emission intensity ratio reaches 0.4:1 (fifth column). The overlaid image of Ect1/E6E7 cells shows an orange red light. The high contrast of the overlaid color between normal and cancer cells suggests that our nanoprobe has high potential for the application in early diagnosis of cancer.

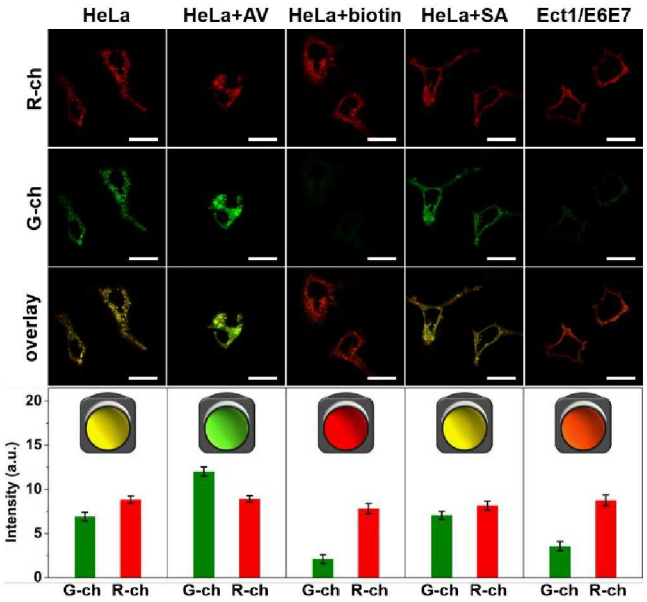

Figure 5. Confocal microscopy images of cervical cells by nanoprobe on (from left to right) HeLa, AV-, biotin-, SA-pretreated HeLa cells, and Ect1/E6E7 cells. Scale bar: 20 μm. Histograms represent cellular emission intensities collected at the green channel (G-ch) and red channel (R-ch). Error bars represent the standard derivation for ten fluorescent foci on cell surface. The traffic lights represent cell surface colors in the overlaid images obtained from red and green emission.

Differentiation of Cancer Cell Types/Subtypes by the Nanoprobe. Accurate differentiation of cancer cell types at a molecular level is highly desirable for diagnostic and therapeutic purposes. By imaging cell surface AV, the traffic light nanoprobe is used to differentiate different cancer cell lines including colon cancer (HCT116), breast cancer (MDA-MB-231 and SKBr3), and hepatoma carcinoma (HepG2) cells. The confocal microscopy images are presented in Figure 6. The red channel emission intensity remains nearly constant, while green channel emission intensity differs among these cells. The obtained relative green-to-red emission intensity ratios are approximately 0.3:1 for HCT116 cells, 0.45:1 for MDA-MB-231 cells, 0.55:1 for SKBr3 cells, and 1:1 for HepG2 cells, respectively. As a result, the overlaid cell images display traffic light-analogous pattern for different types of cancer cells (red for HCT116 cells, orange for MDA-MB-231 cells, yellow for SKBr3 cells and yellowish-green for HepG2 cells, respectively). Notably, MDA-MB-231 and SKBr3 cells, the subtypes of breast cancer cells, can be visually differentiated by the nanoprobe. On the basis of the overlaid colors, expression levels of cell surface AV can be semi-quantitatively assessed to be "-" for HCT116 cells, "+" for MDA-MB-231 cells, "++" for SKBr3 cells and "+++" for HepG2 cells, respectively. Our ratiometric imaging results of cell surface AV for these cancer cell lines are consistent with the results obtained by the flow cytometry method.[48]

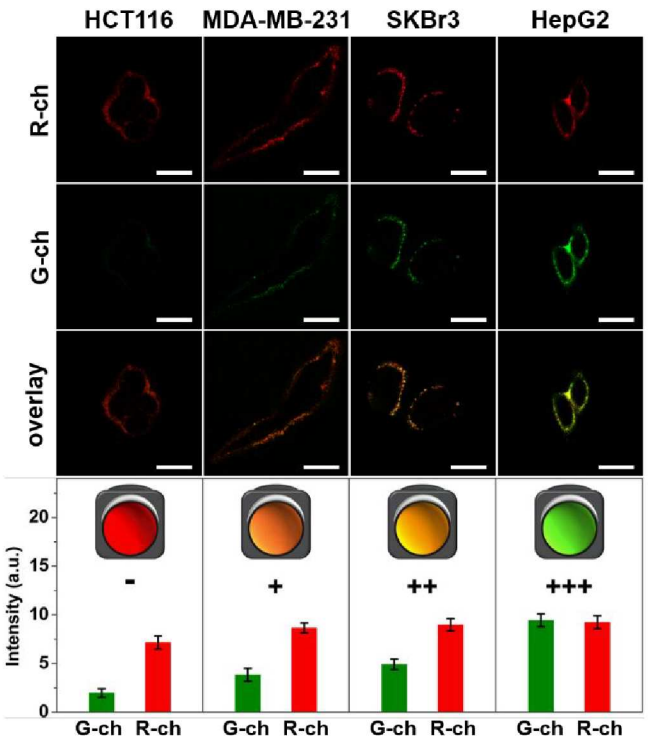

Figure 6. Confocal microscopy images of different types of cancer cells by nanoprobe on (from left to right) HCT116, MDA-MB-231, SKBr3 and HepG2 cells. Scale bar: 20 μm. Histograms show cellular emission intensities collected at the green channel and red channel. Error bars represent the standard derivation for ten fluorescent foci on cell surface. The traffic lights represent cell surface colors in the overlaid images. Symbol of "-" represent BRs-negative cells, and symbols "+", "++", "+++" represent BRs-positive cells with increasing expression levels.

Tracking a Cell Cycle by the Nanoprobe. Knowledge of cell cycles is potentially important to understand the progress of human diseases. Here, the traffic light nanoprobe is further used to examine a cell cycle by tracking the change in expression level of cell surface AV. HeLa cells were pre-treated to obtain the interphase (G1, S, and G2) and the mitosis (M) phase, respectively, followed by treating with the nanoprobe at the preferential condition. The confocal microscopy images are presented in Figure 7. The change in green channel emission during the cell cycle is not obvious. In contrast, the overlaid cell images display a distinguishable color change. With an overlaid color of yellowish-green, the G2 phase can be distinguished from other stages (yellow color). The relative green-to-red emission intensity ratio for G2 phase (0.9:1) is higher than that for G1/S phase (0.6:1), and also higher than that for M phase (0.8:1). With respect to the G1/S phase, the G2 phase involves pronounced cell growth and protein synthesis ahead of mitosis, and therefore necessitates overexpression of BRs (including AV) to acquire biotin. For M phase, due to the cell division, each daughter cell has reduced abundance of AV embedded on the surface.

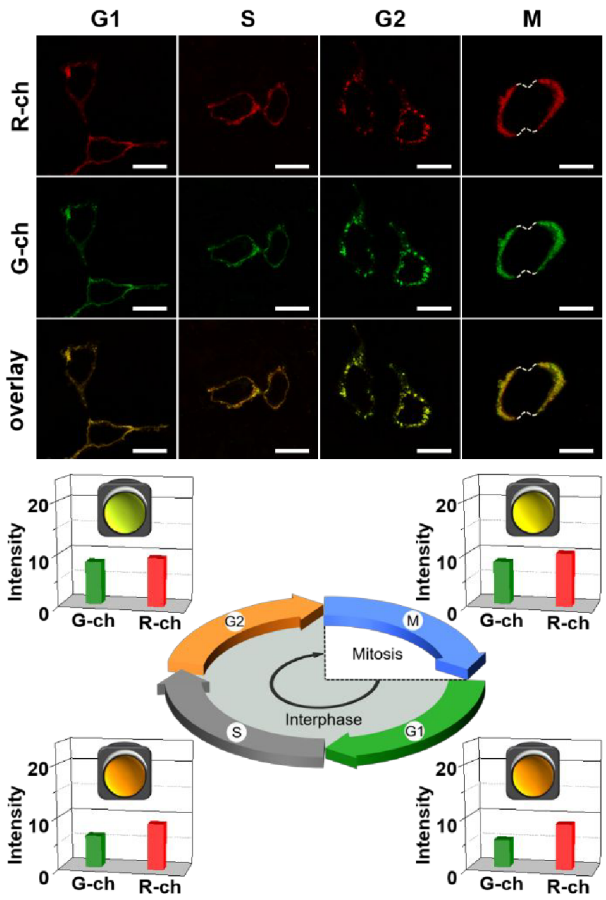

Figure 7. Confocal microscopy images of HeLa cells at different stages of cell cycle by the nanoprobe on HeLa cells at G1, S, G2 and M phases. Scale bar: 20 μm. Histograms show evolution of the relative green-to-red emission intensity in the cell cycle. The traffic lights represent cell surface colors in the overlaid images.

CONCLUSIONS

In conclusion, we present a dual emission ratiometric fluorescent nanoprobe to image biotin receptors on cell surfaces. A "love-hate"-type ligand has been developed to allow specific imaging of cell surface avidin. Confocal images have been studied at red and green channels on different cells and at various phases of cell cycle. We have examined the overlaid images obtained from red and green emission for the cell surfaces. The overlaid color (analogous to traffic light) has been used as an indicator to characterize cell status, types/subtypes and phases. Our ratiometric nanoprobe provides a promising tool with both sensitivity and specificity to image cells for diagnostic and therapeutic uses.

ASSOCIATED CONTENT

Supporting Information.

Conjugation, biocompatibility of the nanoprobe, competition experiment with biotin-C-peptide, and confocal microscopy images of HeLa cells treating with varying concentrations of the nanoprobe for different times. This material is available free of charge via the Internet at http://pubs.acs.org.

AUTHOR INFORMATION

Corresponding Author

*Fax: (86) 25-83792349. E-mail: sunqj@seu.edu.cn

ACKNOWLEDGMENTS

This work is financially supported by the NSFC (Grants: 21775021, 21375015) and priority discipline development program of Jiangsu province.

REFERENCES

(1) Mager, M. D.; LaPointe, V.; Stevens, M. M. Exploring and Exploiting Chemistry at the Cell Surface. *Nat. Chem.* **2011**, *3*, 582-589.

(2) Ali, M. M.; Kang, D. K.; Tsang, K.; Fu, M.; Karp, J. M.; Zhao, W. Cell-Surface Sensors: Lighting the Cellular Environment. *Wiley Interdiscip. Rev.* **2012**, *4*, 547-561.

(3) Christopoulos, A. Allosteric Binding Sites on Cell-Surface Receptors: Novel Targets for Drug Discovery. *Nat. Rev. Drug Discov.* **2002**, *1*, 198-210.

(4) Heo, D. N.; Yang, D. H.; Moon, H. J.; Lee, J. B.; Bae, M. S.; Lee, S. C.; Lee, W. J.; Sun, I. C.; Kwon, I. K. Gold Nanoparticles Surface-Functionalized with Paclitaxel Drug and Biotin Receptor as Theranostic Agents for Cancer Therapy. *Biomaterials* **2012**, *33*, 856-866.

(5) Khajehali, E.; Valant, C.; Jörg, M.; Tobin, A. B.; Conn, P. J.; Lindsley, C. W.; Sexton, P. M.; Scammells, P. J.; Christopoulos, A. Probing the Binding Site of Novel Selective Positive Allosteric Modulators at the M1 Muscarinic Acetylcholine Receptor. *Biochem. Pharmacol.* **2018**, *154*, 243-254.

(6) Jiao, Y.; Yin, J.; He, H.; Peng, X.; Gao, Q.; Duan, C. Conformationally Induced Off–On Cell Membrane Chemosensor Targeting Receptor Protein-Tyrosine Kinases for in Vivo and in Vitro Fluorescence Imaging of Cancers. *J. Am. Chem. Soc.* **2018**, *140*, 5882-5885.

(7) Liu, Y.; Zhou, S.; Tu, D.; Chen, Z.; Huang, M.; Zhu, H.; Ma, E.; Chen, X. Amine-Functionalized Lanthanide-Doped Zirconia Nanoparticles: Optical Spectroscopy, Time-Resolved Fluorescence Resonance Energy Transfer Biodetection, and Targeted Imaging. *J. Am. Chem. Soc.* **2012**, *134*, 15083-15090.

(8) Mizusawa, K.; Takaoka, Y.; Hamachi, I. Specific Cell Surface Protein Imaging by Extended Self-Assembling Fluorescent Turn-on Nanoprobes. *J. Am. Chem. Soc.* **2012**, *134*, 13386-13395.

(9) Tan, X.; Constantin, T. P.; Sloane, K. L.; Waggoner, A. S.; Bruchez, M. P.; Armitage, B. A. Fluoromodules Consisting of a Promiscuous RNA Aptamer and Red or Blue Fluorogenic Cyanine Dyes: Selection, Characterization, and Bioimaging. *J. Am. Chem. Soc.* **2017**, *139*, 9001-9009.

(10) Pal, K.; Sharma, V.; Sahoo, D.; Kapuria, N.; Koner, A. L. Large Stokes-Shifted NIR-Emission from Nanospace-Induced Aggregation of Perylenemonoimide-Doped Polymer Nanoparticles: Imaging of Folate Receptor Expression. *Chem. Commun.* **2018**, *54*, 523-526.

(11) Gao, M.; Su, H.; Lin, G.; Li, S.; Yu, X.; Qin, A.; Zhao, Z.; Zhang, Z.; Tang, B. Z. Targeted Imaging of EGFR Overexpressed Cancer Cells by Brightly Fluorescent Nanoparticles Conjugated with Cetuximab. *Nanoscale* **2016**, *8*, 15027-15032.

(12) Tak, Y. K.; Naoghare, P. K.; Kim, B. J.; Kim, M. J.; Lee, E. S.; Song, J. M. High-Content Quantum Dot-Based Subtype Diagnosis and Classification of Breast Cancer Patients Using Hypermulticolor Quantitative Single Cell Imaging Cytometry. *Nano Today* **2012**, *7*, 231-244.

(13) Ko, H. Y.; Choi, K. J.; Lee, C. H.; Kim, S. A Multimodal Nanoparticle-Based Cancer Imaging Probe Simultaneously Targeting Nucleolin, Integrin $A_v\beta_3$ and Tenascin-C Proteins. *Biomaterials* **2011**, *32*, 1130-1138.

(14) Vesely, D. L.; Kemp, S. F.; Elders, M. J. Isolation of a Biotin Receptor from Hepatic Plasma Membranes. *Biochem. Biophys. Res. Commun.* **1987**, *143*, 913-916.

(15) Vadlapudi, A. D.; Vadlapatla, R. K.; Pal, D.; Mitra, A. K. Biotin Uptake by T47D Breast Cancer Cells: Functional and Molecular Evidence of Sodium-Dependent Multivitamin Transporter (SMVT). *Int. J. Pharm.* **2013**, *441*, 535-543.

(16) Russell-Jones, G.; McTavish, K.; McEwan, J.; Rice, J.; Nowotnik, D. Vitamin-Mediated Targeting as a Potential Mechanism to Increase Drug Uptake by Tumours. *J. Inorg. Biochem.* **2004**, *98*, 1625-1633.

(17) Li, X.; Kim, C. y.; Lee, S.; Lee, D.; Chung, H. M.; Kim, G.; Heo, S. H.; Kim, C.; Hong, K. S.; Yoon, J. Nanostructured Phthalocyanine Assemblies with Protein-Driven Switchable Photoactivities for Biophotonic Imaging and Therapy. *J. Am. Chem. Soc.* **2017**, *139*, 10880-10886.

(18) Sun, Q.; Qian, J.; Tian, H.; Duan, L.; Zhang, W. Rational Design of Biotinylated Probes: Fluorescent Turn-on Detection of (Strept)Avidin and Bioimaging in Cancer Cells. *Chem. Commun.* **2014**, *50*, 8518-8521.

(19) He, Q.; Fan, X.; Sun, S.; Li, H.; Pei, Y.; Xu, Y. Highly Selective Turn-on Detection of (Strept)Avidin Based on Self-Assembled Near-Infrared Fluorescent Probes. *RSC Adv.* **2015**, *5*, 38571-38576.

(20) Sun, Q.; Tian, H.; Qu, H.; Sun, D.; Chen, Z.; Duan, L.; Zhang, W.; Qian, J. Discrimination between Streptavidin and Avidin with Fluorescent Affinity-Based Probes. *Analyst* **2015**, *140*, 4648-4653.

(21) Kong, X.; Dong, B.; Zhang, N.; Wang, C.; Song, X.; Lin, W. A Unique Red-Emitting Two-Photon Fluorescent Probe with Tumor-Specificity for Imaging in Living Cells and Tissues. *Talanta* **2017**, *174*, 357-364.

(22) MacNevin, C. J.; Toutchkine, A.; Marston, D. J.; Hsu, C. W.; Tsygankov, D.; Li, L.; Liu, B.; Qi, T.; Nguyen, D. V.; Hahn, K. M. Ratiometric Imaging Using a Single Dye Enables Simultaneous Visualization of Rac1 and Cdc42 Activation. *J. Am. Chem. Soc.* **2016**, *138*, 2571-2575.

(23) Zhou, L.; Zhang, X.; Wang, Q.; Lv, Y.; Mao, G.; Luo, A.; Wu, Y.; Wu, Y.; Zhang, J.; Tan, W. Molecular Engineering of a TBET-Based Two-Photon Fluorescent Probe for Ratiometric Imaging of Living Cells and Tissues. *J. Am. Chem. Soc.* **2014**, *136*, 9838-9841.

(24) Cen, Y.; Wu, Y. M.; Kong, X. J.; Wu, S.; Yu, R. Q.; Chu, X. Phospholipid-Modified Upconversion Nanoprobe for Ratiometric Fluorescence Detection and Imaging of Phospholipase D in Cell Lysate and in Living Cells. *Anal. Chem.* **2014**, *86*, 7119-7127.

(25) Unger-Angel, L.; Rout, B.; Ilani, T.; Eisenstein, M.; Motiei, L.; Margulies, D. Protein Recognition by Bivalent, 'Turn-on' Fluorescent Molecular Probes. *Chem. Sci.* **2015**, *6*, 5419-5425.

(26) Lo, K. K. W.; Zhang, K. Y.; Leung, S. K.; Tang, M. C. Exploitation of the Dual-Emissive Properties of Cyclometalated Iridium(III)–Polypyridine Complexes in the Development of Luminescent Biological Probes. *Angew. Chem. Int. Ed.* **2008**, *120*, 2245-2248.

(27) Slim, M.; Sleiman, H. F. Ruthenium(II)-Phenanthroline-Biotin Complexes: Synthesis and Luminescence Enhancement Upon Binding to Avidin. *Bioconjugate Chem.* **2004**, *15*, 949-953.

(28) Xie, R.; Battaglia, D.; Peng, X. Colloidal InP Nanocrystals as Efficient Emitters Covering Blue to Near-Infrared. *J. Am. Chem. Soc.* **2007**, *129*, 15432-15433.

(29) Goldman, E. R.; Clapp, A. R.; Anderson, G. P.; Uyeda, H. T.; Mauro, J. M.; Medintz, I. L.; Mattoussi, H. Multiplexed Toxin Analysis Using Four Colors of Quantum Dot Fluororeagents. *Anal. Chem.* **2004**, *76*, 684-688.

(30) Wu, L.; Guo, Q.-S.; Liu, Y.-Q.; Sun, Q.-J. Fluorescence Resonance Energy Transfer-Based Ratiometric Fluorescent Probe for Detection of Zn^{2+} Using a Dual-Emission Silica-Coated Quantum Dots Mixture. *Anal. Chem.* **2015**, *87*, 5318-5323.

(31) Liu, Y. Q.; Ye, M. F.; Ge, Q. Y.; Qu, X. J.; Guo, Q. S.; Hu, X. Y.; Sun, Q. J. Ratiometric Quantum Dot-Ligand System Made by Phase Transfer for Visual Detection of Double-Stranded DNA and Single-Nucleotide Polymorphism. *Anal. Chem.* **2016**, *88*, 1768-1774.

(32) Bharadwaj, V. S.; Dean, A. M.; Maupin, C. M. Insights into the Glycyl Radical Enzyme Active Site of Benzylsuccinate Synthase: A Computational Study. *J. Am. Chem. Soc.* **2013**, *135*, 12279-12288.

(33) Huang, H.; Ji, H.; Li, H.; Jing, Q.; Labby, K. J.; Martásek, P.; Roman, L. J.; Poulos, T. L.; Silverman, R. B. Selective Monocationic Inhibitors of Neuronal Nitric Oxide Synthase. Binding Mode Insights from Molecular Dynamics Simulations. *J. Am. Chem. Soc.* **2012**, *134*, 11559-11572.

(34) Bakalova, R.; Zhelev, Z.; Ohba, H.; Baba, Y. Quantum Dot-Conjugated Hybridization Probes for Preliminary Screening of SiRNA Sequences. *J. Am. Chem. Soc.* **2005**, *127*, 11328-11335.

(35) Liu, B.; Zeng, F.; Wu, G.; Wu, S. A FRET-Based Ratiometric Sensor for Mercury Ions in Water with Multi-Layered Silica Nanoparticles as the Scaffold. *Chem. Commun.* **2011**, *47*, 8913-8915.

(36) Jin, H. J.; Liu, Y. Q.; Xu, T. S.; Qu, X. J.; Bian, F. K.; Sun, Q. J. Quantum Dots–Ligand Complex as Ratiometric Fluorescent Nanoprobe for Visual and Specific Detection of G-Quadruplex. *Anal. Chem.* **2016**, *88*, 10411-10418.

(37) Bencini, A.; Lippolis, V. 1,10-Phenanthroline: A Versatile Building Block for the Construction of Ligands for Various Purposes. *Coord. Chem. Rev.* **2010**, *254*, 2096-2180.

(38) Jung, D.; Maiti, S.; Lee, J. H.; Lee, J. H.; Kim, J. S. Rational Design of Biotin–Disulfide–Coumarin Conjugates: A Cancer Targeted Thiol Probe and Bioimaging. *Chem. Commun.* **2014**, *50*, 3044-3047.

(39) Strzelczyk, P.; Bujacz, A.; Plażuk, D.; Zakrzewski, J.; Bujacz, G. Structural Investigation of the Interactions of Biotinylruthenocene with Avidin. *Chem. Biol. Interact.* **2013**, *204*, 6-12.

(40) Plażuk, D.; Zakrzewski, J.; Salmain, M. Biotin as Acylating Agent in the Friedel–Crafts Reaction. Avidin Affinity of Biotinyl Derivatives of Ferrocene, Ruthenocene and Pyrene and Fluorescence Properties of 1-Biotinylpyrene. *Org. Biomol. Chem.* **2011**, *9*, 408-417.

(41) Loosli, A.; Rusbandi, U. E.; Gradinaru, J.; Bernauer, K.; Schlaepfer, C. W.; Meyer, M.; Mazurek, S.; Novic, M.; Ward, T. R. (Strept)Avidin as Host for Biotinylated Coordination Complexes: Stability, Chiral Discrimination, and Cooperativity. *Inorg. Chem.* **2006**, *45*, 660-668.

(42) Macwan, I.; Khan, M. D. H.; Aphale, A.; Singh, S.; Liu, J.; Hingorani, M.; Patra, P. Interactions between Avidin and Graphene for Development of a Biosensing Platform. *Biosens. Bioelectron.* **2017**, *89*, 326-333.

(43) Weber, P.; Ohlendorf, D.; Wendoloski, J.; Salemme, F. Structural Origins of High-Affinity Biotin Binding to Streptavidin. *Science* **1989**, *243*, 85-88.

(44) Wilchek, M.; Bayer, E. A.; Livnah, O. Essentials of Biorecognition: The (Strept)Avidin–Biotin System as a Model for Protein–Protein and Protein–Ligand Interaction. *Immunol. Lett.* **2006**, *103*, 27-32.

(45) Pazy, Y.; Kulik, T.; Bayer, E. A.; Wilchek, M.; Livnah, O. Ligand Exchange between Proteins. Exchange of Biotin and Biotin Derivatives between Avidin and Streptavidin. *J. Biol. Chem.* **2002**, *277*, 30892-30900.

(46) Fairhead, M.; Shen, D.; Chan, L. K. M.; Lowe, E. D.; Donohoe, T. J.; Howarth, M. Love–Hate Ligands for High Resolution Analysis of Strain in Ultra-Stable Protein/Small Molecule Interaction. *Bioorg. Med. Chem.* **2014**, *22*, 5476-5486.

(47) Louie, M. W.; Ho-Chuen Lam, M.; Kam-Wing Lo, K. Luminescent Polypyridinerhenium(I) Bis-Biotin Complexes as Crosslinkers for Avidin. *Eur. J. Inorg. Chem.* **2009**, 4265-4273.

(48) Ren, W. X.; Han, J.; Uhm, S.; Jang, Y. J.; Kang, C.; Kim, J. H.; Kim, J. S. Recent Development of Biotin Conjugation in Biological Imaging, Sensing, and Target Delivery. *Chem. Commun.* **2015**, *51*, 10403-10418.

For TOC Only